

Electroabsorption spectroscopy of intersubband transitions in multiple-quantum-well superlattices

J. Oiknine-Schlesinger

*Solid State Institute, Technion–Israel Institute of Technology, Haifa 32000, Israel
and Department of Physics, Technion–Israel Institute of Technology, Haifa 32000, Israel*

M. Gerling

Solid State Physics, Lund University, 22100-Lund, Sweden

D. Gershoni and E. Ehrenfreund

*Solid State Institute, Technion–Israel Institute of Technology, Haifa 32000, Israel
and Department of Physics, Technion–Israel Institute of Technology, Haifa 32000, Israel*

D. Ritter

*Solid State Institute, Technion–Israel Institute of Technology, Haifa 32000, Israel
and Department of Electrical Engineering, Technion–Israel Institute of Technology, Haifa 32000, Israel*

(Received 20 May 1999; revised manuscript received 9 December 1999)

We apply intersubband electroabsorption spectroscopy to a current-carrying multiple quantum-well structure device, in order to simultaneously measure the steady state carrier density and the average time carriers spend in each quantum well. By comparing our measurements with a simple quantum mechanical tunneling model, we show directly that electrons sequentially tunnel through the periodic quantum structure. In addition, we use photoinduced absorption spectroscopy to measure the effect of the applied electric field on electron states within the minibands in the energy continuum. We show that already at relatively small fields, the optical transitions into the continuum minibands merge into a single spectral band. Using an eight-band model, we explain this observation in terms of field-induced miniband state localization.

I. INTRODUCTION

The energy spectrum of an ordered array of quantum wells (QW's), separated from each other by a barrier, is composed of allowed minibands and forbidden minigaps.¹ These minibands are formed from the discrete spectrum of the individual QW's due to the overlap between wave functions of neighboring QWs. As a result, the energy width of a particular miniband decreases with the barrier width and increases with the energy of the miniband. It is common to distinguish between the discrete and the continuous part of the spectrum at energies below the barrier potential and above it, respectively. In the first part, the carrier wave functions are strongly localized, their overlap is negligible, and the energy minibands are almost discrete. In the latter part, the wave function overlap is considerable and the carrier wave functions are coherent over many periods. The energy spectrum is then composed of minibands that are separated by forbidden minigaps. At even higher energies, these minibands become wider, the minigaps shrink, and the spectrum becomes continuous. In Fig. 1(a) we present the calculated dispersion curves for a multiple-quantum-well (MQW) structure, where each period is composed of a 6 nm thick $\text{In}_x\text{Ga}_{1-x}\text{As}$ QW and a 30-nm-thick InP barrier [Fig. 1(b)]. The band structure displayed in Fig. 1(a) consists of two confined levels ($e1$ and $e2$), with energies below the barrier potential, and a set of minibands (C_n , $n = 3, 4, \dots$) with energies above the barrier. The calculated intersubband absorption spectrum of such a structure with electron population in its $e1$ level is presented in Fig. 1(c). We note that the absorption due to optical transitions between the confined states, $e1$ - $e2$, is much stronger

than that due to transitions between $e1$ and the continuum minibands C_n . In previous studies we reported on the observation of these continuum minibands^{2,3} by means of optical absorption due to optical transitions from $e1$ occupied electron states to “empty” electron states in the minibands. In this work we apply bias to an undoped periodic MQW structure, embedded between two n -doped semiconducting regions (a n - i - n device). We simultaneously measure the current and intersubband absorption under bias application. Thereby, we study both the effects of the electric field on the MQW continuum minibands and the tunneling of carriers through the periodic potential. We demonstrate that the continuum minibands are dramatically affected by the application of relatively small electric fields. This is qualitatively explained in terms of field induced miniband electron wave function localization.^{4,5} The magnitude of the effect is quantitatively accounted for by our eight-band $\mathbf{k}\cdot\mathbf{p}$ model. The ability to simultaneously measure both the current and the induced intersubband absorption in our specially fabricated device allows us to evaluate the carrier tunneling times directly. These, in turn, are favorably compared with estimates based on simple quantum mechanical calculations with no scattering.

II. EXPERIMENTAL DETAILS

The device we used contains a MQW embedded within the intrinsic region of a n - i - n structure. It was grown by metalorganic molecular beam epitaxy⁶ on a semi-insulating (100)-oriented InP substrate. The MQW contains 25 periods

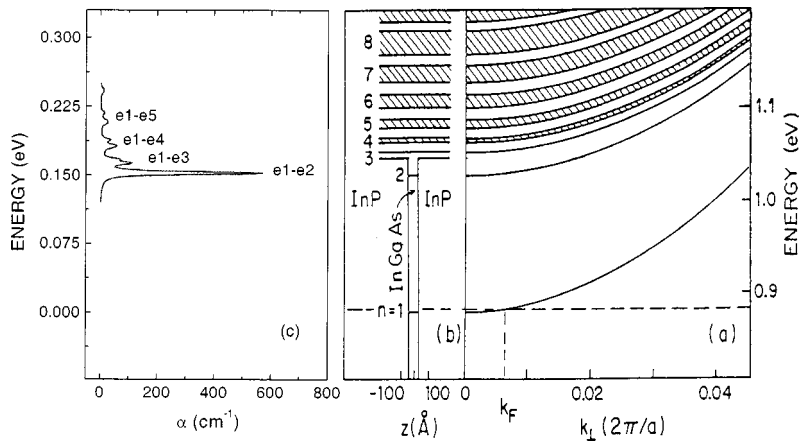


FIG. 1. (a) Calculated conduction subband dispersion curves vs the in-plane wave vector k_{\perp} for the $\text{In}_{0.53}\text{Ga}_{0.47}\text{As}$ MQW shown in (b). The dashed horizontal line marks the Fermi energy for which the calculated intersubband absorption is shown in (c). (b) Real space representation of one period of the MQW. $n=1$ and 2 correspond to the confined energy levels $e1$ and $e2$, respectively. $n=3, 4, \dots$ correspond to the continuum minibands C_n . (c) The calculated intersubband absorption spectra of the device.

of 6-nm-thick $\text{In}_{0.53}\text{Ga}_{0.47}\text{As}$ QW and 30-nm-thick InP barrier in each period. The device is schematically described in Fig. 2. The top contact layer is a 90 nm thick $5 \times 10^{18} \text{ cm}^{-3}$ Sn-doped $\text{In}_{0.53}\text{Ga}_{0.47}\text{As}$ layer capped by an 80-nm-thick InP cap layer. The bottom contact layer is a 370-nm thick Sn-doped $\text{In}_{0.53}\text{Ga}_{0.47}\text{As}$ layer separated from the intrinsic region by a 200-nm-thick InP buffer layer. The layer dimensions and compositions were determined by high-resolution x-ray diffraction measurements.

The device is biased by two metal electrodes A and B that were deposited on the top and bottom contact layers, respectively, using standard photolithographic techniques. The sample was prepared as a multipass waveguide for the infrared radiation by polishing its sides at a 45° angle (Fig. 2), enabling intersubband absorption measurements using a p -polarized infrared beam.²

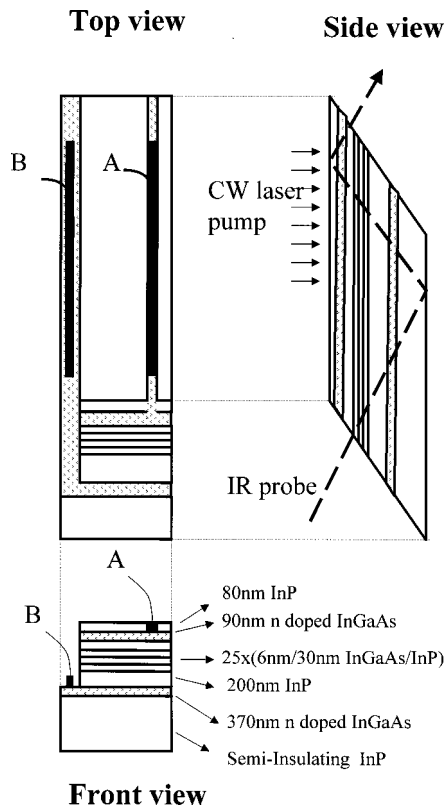


FIG. 2. Schematic description of the device under study. Its top, front, and side views are shown. The metal wires A and B are connected to the top and bottom contact layers, respectively.

The electroabsorption (EA) and photoinduced absorption (PIA) spectra were obtained by measuring the changes in the intersubband absorption due to modulation of the applied voltage and the interband exciting laser beam, respectively. The nominal electric field due to the applied voltage V is determined from the sample geometry and is given by $F = V/d$, where $d = 1.4 \mu\text{m}$ is the effective width of the intrinsic region along the field direction. For PIA we used the 514.5 nm Ar^+ line as the pump beam, which was modulated at ≈ 1.6 kHz. This modulation frequency is orders of magnitude slower than the excess carrier recombination and tunneling rates (see below) and thus only the in-phase modulation signal was considered.⁷ We used a step-scan Fourier transform infrared (FTIR) spectrometer, with a Nernst glower as the probe beam, where the modulated signals were measured using a lock-in technique. For the PIA measurements, the phase was fixed by allowing part of the pump beam to be detected directly by the detector. We note here that in the process of Fourier transforming the measured transmission signal, the sign of the measured signal is lost, and the deduced differential absorption spectrum is always positive. We determined the actual sign of the measured differential spectra utilizing a sign-sensitive monochromator setup.⁸ Unless otherwise noted, the data presented below are corrected for the sign of the modulated absorption. For the EA measurements the phase was nullified directly on the signal, since we verified by the sign-sensitive setup that it is in phase and increases with the applied voltage. All measurements were done at low temperatures around 6 K.

III. CURRENT-INDUCED INTERSUBBAND ABSORPTION BETWEEN CONFINED ELECTRON STATES

A. Determination of the carrier density during current injection

The application of a bias ($V \equiv V_A - V_B$) to the terminals of our monopolar device (Fig. 2) results in two simultaneous effects: (a) Electric field is being built in the intrinsic region of the device along the superlattice growth direction; (b) Electrons are injected into the intrinsic region and then tunnel through the barriers of the potential structure. The first effect influences mainly the spectral shape of the absorption, while the second determines mainly its magnitude. We use these features of the intersubband EA in order to gain better understanding of the processes by which the electrons tunnel into and are captured by the QW's.

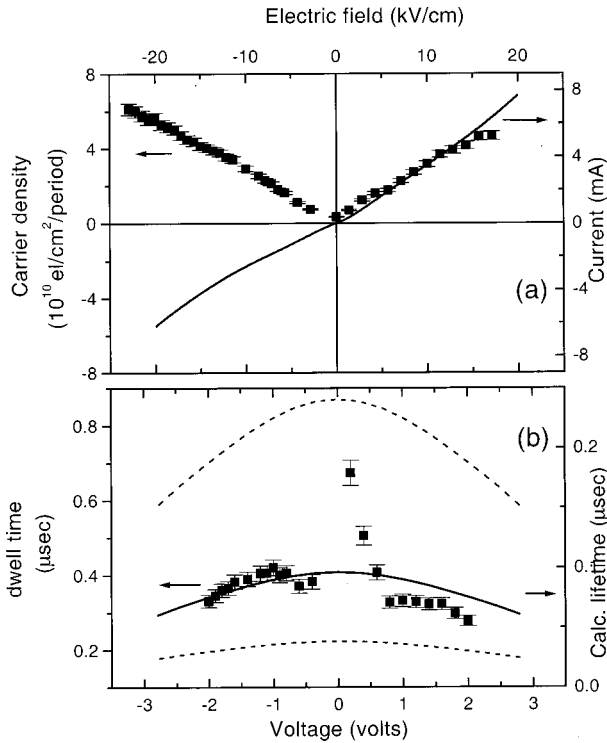


FIG. 3. (a) Solid line: Dark current vs voltage (I - V) curve of the device. The symbols represent the corresponding carrier densities deduced from the measured intersubband absorption spectra. The top scale displays the electric field as estimated from the applied voltage and the sample dimensions. (b) Calculated (solid line) and measured (symbols) electron tunneling times vs the applied bias V . The measured times were deduced using Eq. (1). The top and bottom dashed lines represent the uncertainty in the calculated times due to 1 monolayer structural and 1% compositional uncertainty.

In Fig. 3(a) (right axis, solid line) we present the I - V characteristics of the device. The current through the device is nearly proportional to the voltage applied to it. This clearly indicates that the electric contacts are ohmic. In Fig. 4 we show a set of EA spectra for various bias voltages applied to the device. EA spectra that were obtained under negative (i.e., $V_A < V_B$) and positive (i.e., $V_A > V_B$) voltage modula-

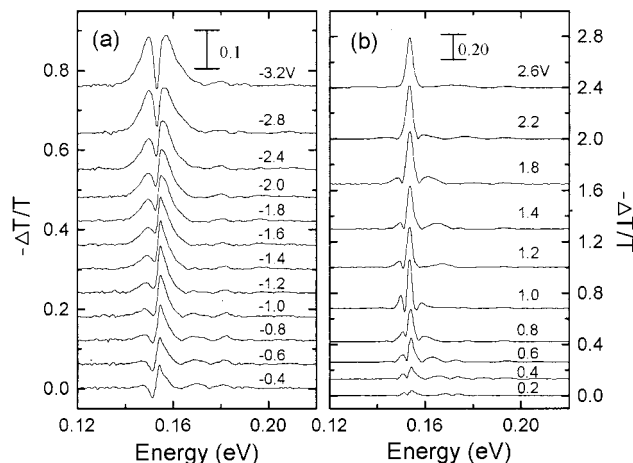


FIG. 4. Absolute value of EA spectra for negative (a) and positive (b) bias applied to the device, as measured in the FTIR spectrometer (see Sec. II).

tions are presented in Figs. 4(a) and 4(b), respectively. The spectra in Fig. 4 display the absolute value of the modulated EA signals, directly as measured by the FTIR (see Sec. II). The main spectral feature observed at ≈ 153 meV is due to the $e1$ - $e2$ optical transition between the two confined electron states. The spectral position of this transition is almost independent of the applied bias. In particular, the expected spectral blue shift of the $e1$ - $e2$ transition^{9,10} is not observed. This indicates that the electric field in the intrinsic region of the device is quite small (≤ 20 kV/cm, see below). Thus, the observed changes in the EA spectra must be due to the voltage-induced electron current through the device.

The EA signal increases with applied voltage for both polarities. Since our lock-in modulated technique measures only the changes in absorption due to the bias voltage, direct integration of the EA spectra yields the net integrated absorption due to the voltage-induced current. At each bias voltage, the added steady-state electron density was then quite accurately extracted from the $e1$ - $e2$ absorption band by comparing it with our eight-band $\mathbf{k} \cdot \mathbf{p}$ optical absorption model calculations.¹¹ The carrier densities thus obtained are presented in Fig. 3(a) as the solid squares. We note that the electron density is an increasing function of the injected current. The ability to directly correlate the accumulated electron density in the QWs, as independently measured by the intersubband absorption, with the measured electron current is unique to our technique. We can accurately determine the average QW carrier density for a given current through the device. We use this ability in order to obtain the average time that an electron spends within the superlattice. This important quantity is usually estimated using various assumptions and models in which the electron ‘‘capture time’’ is indirectly extracted from the experimental results.^{12,13}

The data presented in Fig. 3(a) imply a one to one correspondence between the electron density in the first level of the QW’s ($e1$) and the current I through the device. If we denote by τ the time that an electron spends in the MQW structure, the following relation applies:

$$J = N/\tau, \quad (1)$$

where $J = I/eA$ is the electron flux density, A is the area of the device cross section, and N is the electron sheet density. Using the experimental data presented in Fig. 3(a) and Eq. (1) we calculated τ . The results are plotted in Fig. 3(b) (left axis, symbols) as τ vs the bias voltage V . For negative bias, τ is ≈ 0.4 μ sec at low absolute bias, and it slightly decreases as $|V|$ increases. Similar behavior is observed for positive bias, except for $V < 0.6$ V, where an abrupt increase in τ is observed as $V \rightarrow 0$.

Since the measurements were performed at low temperatures (6 K), the only effective transport mechanism to be considered is tunneling. This means that with the application of an external electric field the tunneling becomes easier. We theoretically estimated the effect of the external field on the tunneling by calculating the lifetime of the $e1$ level. This was done in the following way. We first calculated the transmission probability of an electron through the periodic structure under an applied electric field using the resonant tunneling method.¹⁴ In the calculations we included the electron mass dependence on the energy (band nonparabolicity).¹⁵ The transmission probability as a function of energy shows

typical resonances associated with the electron levels and minibands. The full width at half the resonance maximum, Γ , yields the resonance level lifetime, $\tau = \hbar/\Gamma$. Therefore, the $e1$ level lifetime is the time that an electron spends on average within the MQW structure before it tunnels out of it. In reality, this description is valid as long as the electronic wave function is coherent along the whole structure. The electronic coherence length is limited, however. In particular, in the presence of a large electric field, it may not exceed more than one or two periods. This means that the lifetime calculated above represents only the dwell time for an electron within the MQW part in which its wave function is coherent. Phrasing it differently, this means that electron tunneling across the MQW is essentially a sequential process, and not a coherent one. Therefore, the τ calculated above represents the dwell time for electrons in a single QW. In Fig. 3(b) (right axis) we present by the solid line the calculated dwell times as a function of the applied voltage on the MQW structure, assuming that the voltage drops entirely within the intrinsic region of our device. The dashed lines in Fig. 3(b) mark the uncertainties in our calculations, assuming ± 1 monolayer uncertainty in the MQW structure and 1% uncertainty in its QW composition. For comparison, we display by squares in Fig. 3(b) (left axis) the experimentally deduced dwell times. Surprisingly, our calculations yield times that are roughly a factor of 4 shorter than the experimentally deduced ones. This may result from an inhomogeneous current distribution in our device, which leads to a smaller effective device area. We conclude that by simultaneous measurements of the current through a quantum structure and the intersubband absorption that is induced by this current, one can estimate the time that carriers spend within the quantum structure. At low temperatures, these dwell times are in reasonable agreement with simple quantum mechanical tunneling calculations.

B. Line shapes and linewidths

We now turn to discuss the current and polarity dependence of the intersubband EA line shape. For positive bias voltage ($V_A > V_B$) the width and the spectral shape of the EA are nearly independent of the bias voltage and injected currents. In contrast, negative bias changes the line shape and its spectral width considerably. In order to quantify these spectral changes we used a two-Gaussian-line fit to the measured spectra. In Fig. 5 we describe the fitting procedure. The negative dotted Gaussian in Fig. 5 represents the absorption signal due to residual electrons within the MQW structure, when no bias is applied to the device, and no current flows across it. The positive dotted Gaussian represents the fitted current-induced absorption. The dotted-dashed line represents the sum of the two Gaussians that best fitted the EA spectrum (solid line). We see from these fits to EA spectra under various biases that the polarity dependence of the line shape is mostly due to bias-induced $e1-e2$ transition energy redshifts and line broadening. In Fig. 6 we display the width of the current-induced intersubband absorption thus extracted, as a function of the bias. A significantly broader linewidth at negative bias is clearly seen. The linewidth increases from ≈ 3 meV at zero bias to ≈ 13 meV at -3 V. In spite of this drastic difference between the cases of positive

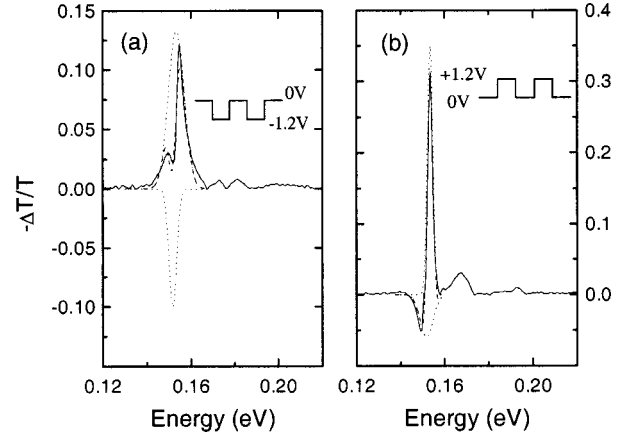


FIG. 5. EA spectra for negative (a) and positive (b) device bias. For each polarity, the solid line represents the measured spectrum (including the sign, see Sec. II), the positive (negative) dotted line represents a single Gaussian fit to the biased (zero bias) spectrum, and the dotted-dashed line is the algebraic sum of the two Gaussians that best fitted the measured EA.

and negative bias, we note that the area under the EA curves is practically polarity independent [Fig. 3(a), left axis]. This proves, as expected, that the current-induced steady-state QW electron population depends only on the current magnitude, and not on its direction. We attribute the bias polarity linewidth dependence to the structural asymmetry of the $n-i-n$ device. Whereas for negative bias, electrons must get through a 200-nm-thick InP barrier before they reach the MQW region, for positive bias they tunnel only through a 30-nm-thick barrier. Therefore, the electrons are injected into the MQW region with much higher kinetic energy when the device is under negative bias. The electrons are thus effectively “hotter” for negative bias and they occupy higher in-plane momentum states. Due to the electron mass nonparabolicity, the $e1-e2$ intersubband transition occurs at lower energies for higher in-plane momentum states. Thus, hotter carriers give rise to intersubband line broadening with a characteristic lower energy tail, similar to the experimental observations (Fig. 4). We note here the similar broadening of the $e1-e2$ transitions observed as the temperature is raised.¹⁶

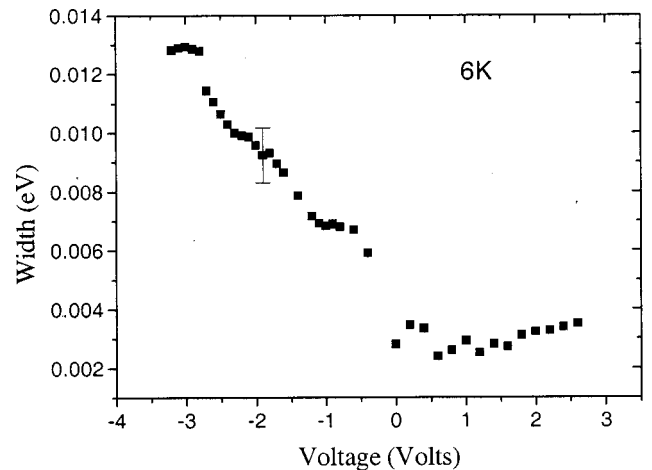


FIG. 6. The linewidth of the current-induced $e1-e2$ intersubband absorption vs the applied bias voltage.

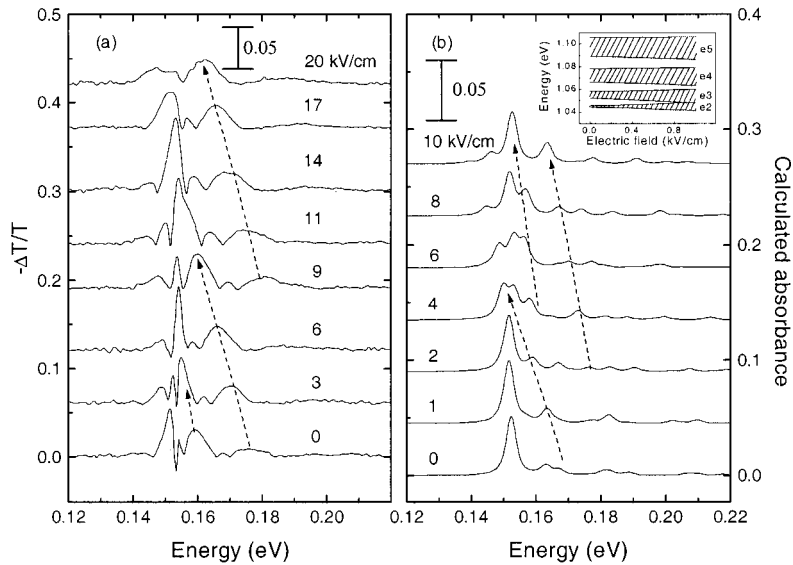


FIG. 7. (a) Measured PIA under various positive bias voltages. The electric-field values were extracted using the sample dimensions, as explained in the text. (b) Calculated intersubband absorption for various applied fields and at fixed carrier density of $5 \times 10^{16} \text{ cm}^{-3}$. The inset shows the calculated evolution of the minibands with the applied electric field. The tilted arrows in both (a) and (b) indicate the redshifted $e1-C_n$ optical transitions.

IV. CONFINED TO CONTINUUM ELECTROABSORPTION

In addition to the strong $e1-e2$ absorption peak, the intersubband absorption spectrum of MQW's contains also weaker absorption peaks at higher energies. These absorption peaks, due to optical transitions of electrons from the confined $e1$ level to the continuum minibands,² are clearly observed in the EA spectra of Fig. 4. Unlike the confined to confined ($e1-e2$) intersubband transition energy, the confined to continuum ($e1-C_n$) transition energies decrease rapidly with the applied electric field. They merge with the $e1-e2$ transition already at an electric field of $\approx 20 \text{ kV/cm}$. This effect is more clearly seen in the photoinduced intersubband absorption spectra for various applied electric fields, as shown in Fig. 7. In Fig. 7(a) we present the measured PIA spectra excited with the 514.5 nm Ar^+ laser line, for various bias voltages. It is apparent that already at very low applied fields ($< 5 \text{ kV/cm}$) a substantial decrease in the energy of the intersubband transitions to the continuum minibands is observed. This trend increases with further increase in the applied field, as is clearly seen in Fig. 7(a). The dashed arrows in Fig. 7(a) mark the spectral evolution of three $e1-C_n$ transitions, with the increase of the applied electric field. The optical transition energies are redshifted with the electric field, eventually merging into a "single," relatively broad, transition, very close to the nearly unshifted $e1-e2$ transition. We note here that the data presented in Fig. 7(a) were taken with positive bias voltage. Qualitatively similar behavior was observed for negative bias or while pumping with $1.06 \mu\text{m}$ laser light (for which the InP layers are transparent) under either bias polarity.

In Fig. 7(b) we present the calculated EA spectra for comparison with the measured data. For the calculations we utilize an eight-band $\mathbf{k} \cdot \mathbf{p}$ method as detailed earlier.¹⁰ The calculations were carried out for a periodic structure of MQW's having the same dimensions and compositions as in the present device. The broadening of the minibands due to the electric field is shown in the inset to Fig. 7(b) where the energy level $e2$, together with the next three higher continuum minibands are plotted as a function of the applied field. The inset demonstrates that at $\approx 1 \text{ kV/cm}$ the electric field has already caused a considerable broadening and mix-

ing of the electronic minibands. This broadening and miniband mixing can be qualitatively understood in terms of Stark ladder formation and field-induced localization of the continuum electron wave functions.^{4,5}

Our calculations describe semiquantitatively the rate at which the various transitions shift to the red with the increase in bias, as well as the order of appearance of the spectral lines. The similarity of the calculated to the measured linewidths of the various transitions and their relative intensities is of a lesser quality, however. This is probably due to the inhomogeneous broadening and the finite electron coherence length, which we do not consider in our calculations.

V. SUMMARY

We have demonstrated an experimental method for measuring the steady-state carrier density in a quantum structure *while* current is flowing through it. The method is based on measurements of the intersubband absorption induced by the current itself. Since at low temperatures the current is solely due to resonant tunneling, the method allows determination of the actual dwell time that carriers spend in the structure. By comparing our experimental measurements with a simple quantum-mechanical tunneling model, we conclude that the coherence length of electrons in the MQW structure that we study does not exceed more than one or two periods. Consequently, the tunneling process must be sequential.

We also measured the intersubband electroabsorption due to optical transitions to the continuum minibands. We show that the energy position and the intensity of these transitions are very sensitive to an externally applied electric field. We quantitatively account for this behavior in terms of a theory that naturally includes the effects of field-induced Stark ladder formation and miniband wave-function localization.

ACKNOWLEDGMENTS

This work was supported by the Israel Science Foundation founded by the Israel Academy of Sciences and Humanities, and by the fund for promotion of research at the Technion.

- ¹G. Bastard, *Wave Mechanics Applied to Semiconductor Heterostructures* (Les Edition de Physique, Paris, 1988), Chap. III.
- ²D. Gershoni, J. Oiknine-Schlesinger, E. Ehrenfreund, D. Ritter, R. A. Hamm, and M. B. Panish, *Phys. Rev. Lett.* **71**, 2975 (1993).
- ³J. Oiknine-Schlesinger, D. Gershoni, E. Ehrenfreund, D. Ritter, R. A. Hamm, J. M. Vandenberg, and S-N. G. Chu, *Solid-State Electron.* **37**, 1269 (1994).
- ⁴E. E. Mendez, F. Agullo-Rueda, and J. M. Hong, *Phys. Rev. Lett.* **60**, 2426 (1988).
- ⁵J. Bleuse, G. Bastard, and P. Voisin, *Phys. Rev. Lett.* **60**, 220 (1988).
- ⁶D. Ritter, R. A. Hamm, M. B. Panish, J. M. Vandenberg, D. Gershoni, S. D. Gunapala, and B. F. Levine, *Appl. Phys. Lett.* **59**, 552 (1991).
- ⁷E. Dekel, E. Ehrenfreund, D. Gershoni, and P. Boucaud, *Phys. Rev. B* **56**, 15 734 (1997).
- ⁸J. Oiknine-Schlesinger, E. Ehrenfreund, D. Gershoni, D. Ritter, M. B. Panish, and R. A. Hamm, *Appl. Phys. Lett.* **62**, 970 (1991).
- ⁹A. Harwit and J. S. Harris, *Appl. Phys. Lett.* **50**, 685 (1987); *J. Appl. Phys.* **60**, 3211 (1990).
- ¹⁰M. E. Pistol and D. Gershoni, *Phys. Rev. B* **50**, 11 738 (1994).
- ¹¹D. Gershoni, C. Henry, and J. Baraff, *IEEE J. Quantum Electron.* **29**, 2433 (1993).
- ¹²B. F. Levine, K. K. Choi, C. G. Bethea, J. Walker, and R. J. Malik, *Appl. Phys. Lett.* **50**, 1092 (1987).
- ¹³See the review paper by B. F. Levine, *J. Appl. Phys.* **74**, R2 (1993).
- ¹⁴D. A. B. Miller, D. S. Chemla, T. C. Damen, A. C. Gossard, W. Wiegmann, T. H. Wood, and C. A. Burrus, *Phys. Rev. B* **32**, 1043 (1985).
- ¹⁵D. Gershoni, H. Temkin, M. B. Panish, and R. A. Hamm, *Phys. Rev. B* **39**, 878 (1989).
- ¹⁶D. Gershoni, R. Duer, J. Oiknine-Schlesinger, E. Ehrenfreund, D. Ritter, R. A. Hamm, J. M. Vandenberg, and S.-N. G. Chu, in *Quantum Well Intersubband Transitions—Physics and Devices*, edited by H. C. Liu *et al.* (Kluwer, Dordrecht, 1994), pp. 275–289.